[12]K. O. Groneveld, B. Hubert, R. Bass, and H. Nann, Nucl. Phys. A151, 198 (1970).
[13]M. W. Greene, C. C. Green, and G. D. Jones, Phys. Letters 32B, 680 (1970).
[14]J. R. Erskine, D. J. Crozier, J. P. Schiffer, and W. P. Alford, Phys. Rev. C 3, 1976 (1971).
[15]M. C. Bouten, J. P. Elliott, and J. A. Pullen, Nucl. Phys. A97, 113 (1967).
[16]P. Wasielewski and F. B. Malik, Nucl. Phys. A160, 113 (1971).
[17]D. Evers and W. Stocker, Phys. Letters 33B, 559 (1970).
[18]H. D. Graber and G. I. Harris, Phys. Rev. 188, 1685 (1969).
[19]K. W. C. Stewart, B. Castel, and I. P. Johnstone, to be published.
[20]A. K. Hyder and G. I. Harris, private communication.

PHYSICAL REVIEW C VOLUME 5, NUMBER 5 MAY 1972

Neutron-Gamma Competition Following (d, d') Reactions*

C. Ling,† D. Bodansky, J. R. Calarco,‡ and J. M. Cameron§
Department of Physics, University of Washington, Seattle, Washington 98195
(Received 3 February 1972)

The $(d,d'n)$ reaction has been studied in ^{61}Ni and other targets, using 19-MeV deuterons. Deuteron angular distributions and yields indicate that the (d,d') reaction is predominantly direct at forward angles, but probably has a large compound-nuclear component at backward angles, and observed angular correlations for d'-n coincidences indicate that the neutrons are mainly products of evaporation from a ^{61}Ni compound nucleus. The fractional yield, $F_n = \Gamma_n/\Gamma$, for neutron emission is found to be substantially below unity for ^{61}Ni excitation energies E_i extending to several MeV above the neutron binding energy B_n (e.g., $F_n \cong 0.75$ at $E_i - B_n = 2$ MeV), indicating the importance of competition from γ-ray emission. For $E_i - B_n < 3$ MeV, F_n is independent of deuteron angle and its magnitude can be accounted for in terms of the statistical model. Because the relative neutron and γ-ray emission widths are strongly dependent on the ^{61}Ni spin population, this lack of dependence of F_n on deuteron detection angle suggests that the ^{61}Ni spin population is similar for direct and compound-nuclear (d,d') reactions. For $E_i - B_n > 3$ MeV, the value of F_n at forward deuteron angles is anomalously low. Results are also presented for the $(d,d'n)$ reaction in ^{25}Mg, ^{57}Fe, ^{91}Zr, and ^{119}Sn.

I. INTRODUCTION

The present investigation is concerned with the competition between neutron and γ-ray emission from excited nuclei. In considering compound-nuclear decay, this competition has sometimes been neglected, with the explicit or tacit assumption that neutron emission would be overwhelmingly dominant. The neglect of the role of γ-ray emission at excitation energies above the neutron binding energy was probably influenced by results of slow neutron capture. However, these reactions are selective in populating states which can readily decay by s-wave neutron emission. The situation becomes very different when the compound-nuclear spin is such that neutron decay can only occur with high orbital angular momentum, and there, even for neutron energies of several MeV, the γ yields may compete strongly with neutron emission.

Although sometimes ignored, the role of angular momentum in neutron-γ competition has been studied by a number of authors, especially in the context of the high angular momenta involved in α-particle and heavy-ion bombardments.[1-5] Recently, Cohen *et al.*[6,7] have studied this competition in $(p, p'n)$ reactions. Neutron yields from this reaction, which at first seemed anomalously low, were explained in terms of angular momentum effects,[7] and important qualitative features of the data could be accounted for by the statistical model. Nevertheless, many disagreements with the statistical model were reported in detailed aspects of the results. Interpretation was made particularly difficult because of the ambiguity in distinguishing between events in which the emitted proton came before the neutron and those in which it came after.

This ambiguity is largely removed if one studies $(d, d'n)$ rather than $(p, p'n)$ reactions. If a neutron and deuteron are emitted sequentially, it is highly probable that the deuteron will precede the neutron, rather than follow it. As discussed in more detail in Sec. V, this is a consequence of the low probability of deuteron evaporation from compound nuclei of low excitation energy. On the oth-

er hand, this advantage of $(d, d'n)$ reactions for the study of compound-nuclear competition is to some extent balanced by the fact that the (d, d') reaction is itself largely direct, and it is not *a priori* obvious that coincident neutrons will be evaporation products, rather than partners to the deuterons in some nonstatistical process. Further, if a compound residual nucleus is formed following a direct (d, d') reaction, there is no clear way to use a direct-interaction model to calculate the angular momentum distribution of the compound nuclei and the relative neutron and γ yields. It thus becomes central to this approach to determine the extent to which a compound residual nucleus is formed in the (d, d') reaction and, if one is formed, the extent to which the statistical model can account for the compound-nuclear spin distribution.

If it can be established that the statistical model is appropriate, then the experimental results, given sufficient precision, can provide information on statistical-model parameters, such as nuclear moments of inertia and emission widths for neutrons and γ rays. Conversely, if one believes that these parameters are moderately well known, then the experiment can be viewed as being primarily an exploration of broad features of the reaction mechanism. As will be seen, the more interesting implications of the data relate to the latter issue.

The experimental procedure consisted of bombarding targets, primarily ^{61}Ni, with deuterons, and observing deuterons and neutrons in coincidence. The targets were chosen for relatively low neutron binding energies and for good separation between the ground state and excited states in the final nucleus. Assuming, for the sake of definiteness, a ^{61}Ni target, the (d, d') reaction produces excited ^{61}Ni nuclei with excitation energies defined by the d' energy (see Fig. 1). By appropriate selection of the d' energy, a region of ^{61}Ni excitation energy was chosen where neutron emission is possible, but charged-particle emission is either impossible or greatly inhibited by the Coulomb barrier. The observed coincidence neutron yield, normalized to the inelastic cross section, served to determine the fraction of ^{61}Ni decays which proceed by neutron emission, and hence the relative neutron- and γ-ray-emission probabilities. These deuteron-neutron coincidence measurements were supplemented by deuteron-γ-ray coincidence measurements, which served mainly to confirm the neutron data.

Details of the experimental arrangement are described in Sec. II and details of the procedures for analyzing the data are described in Sec. III. Section IV describes studies of (d, d') spectra which were carried out to explore the (d, d') reaction mechanism. The $(d, d'n)$ coincidence results are described and discussed in Sec. V, and the overall results are summarized in Sec. VI. Details of the statistical-model formalism used in the analysis are presented in the Appendix.

II. EXPERIMENTAL ARRANGEMENT

The experiment was performed using 19-MeV deuterons from the University of Washington three-stage Van de Graaff accelerator. After momentum analysis, the deuteron beam was focused on self-supporting strip targets of ^{61}Ni (92% enriched), ^{57}Fe (91% enriched), ^{25}Mg (99.2% enriched), ^{91}Zr (92% enriched), and ^{119}Sn (90% enriched). The target thicknesses ranged from 0.9 to 2.0 mg/cm^2. Strip targets were used to minimize the kinematic effects of shifts in the beam position over the face of the target. The target was placed at the center of a thin-walled 10-in.-diam spherical aluminum scattering chamber equipped with two movable arms for mounting detectors. The thin walls (50 mil) and absence of massive structures close to the chamber reduced both background radiation and the possibility of neutron rescattering. A schematic of the experimental arrangement is shown in Fig. 2.

Deuterons were detected in a telescope consisting of three solid-state detectors, placed with its defining aperture 2 in. from the target. The first

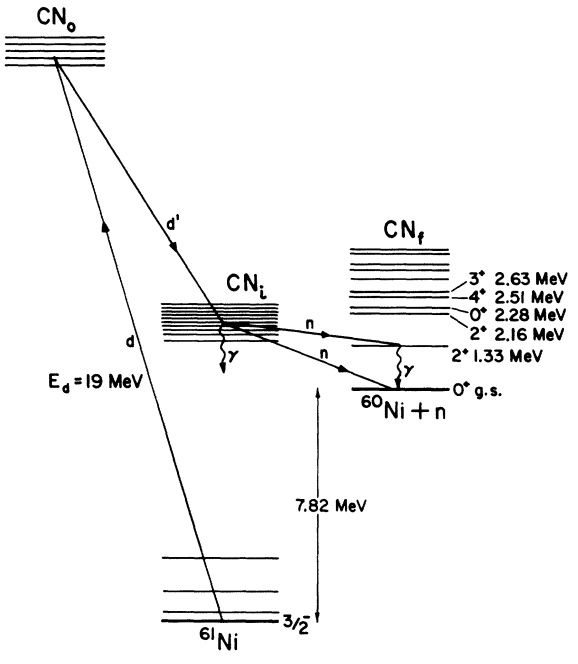

FIG. 1. Energy level diagrams for the reactions ^{61}Ni-$(d, d'n)^{60}$Ni and ^{61}Ni$(d, d'\gamma)^{61}$Ni.

two counters were 300-mm^2 surface-barrier detectors, 100 and 300 μm thick, chosen to observe inelastically scattered deuterons of 4–14 MeV. Particle identification was performed with these two detectors, and the third detector was used for anticoincidence rejection of energetic protons and deuterons. The telescope subtended an angle of 11.4°; consequently there was large kinematic broadening. The over-all resolution (full width at half maximum) was reduced from about 180 to about 120 keV by placing an aluminum foil stack, which had three thickness steps, in front of the detector, such that the thickest part was at the smallest deuteron scattering angle.

Neutrons were detected in a 5-in.-diam-by-1-in.-thick encapsulated NE-213 liquid scintillator viewed by an RCA 4522 photomultiplier. Pulse-shape discrimination (PSD) was used to help reject γ rays, and further γ reduction was achieved by placing $\frac{1}{4}$ in. of lead in front of the scintillator. The neutron counter was placed at a distance of 12 in. from the target. Neutron energies were determined by time of flight (TOF) with respect to associated deuterons. The time resolution of the system, as determined by observing deuteron-γ coincidences, was 1.5 nsec. Typical neutron transit times through the detector were also about 1.5 nsec.

In order to determine the neutron yield quantitatively, an absolute efficiency calibration was made using the associated particle technique.[8] Neutrons and ^{3}He ions from the reaction ^{3}H(p, n)-^{3}He were detected in coincidence, again using the experimental arrangement of Fig. 2, with the ^{3}He counter alone defining the solid angle. In such a geometry, the efficiency of the neutron counter is the ratio of n-^{3}He coincidences to ^{3}He singles. The efficiency with the lead γ-ray absorber in place was measured for neutron energies from 0.75 to 3.0 MeV and is displayed in Fig. 3. A threshold was set at the level of the pulse height of the photopeak of the 60-keV γ ray from ^{241}Am, corresponding to a neutron energy of approximately 0.5–0.6 MeV.[9]

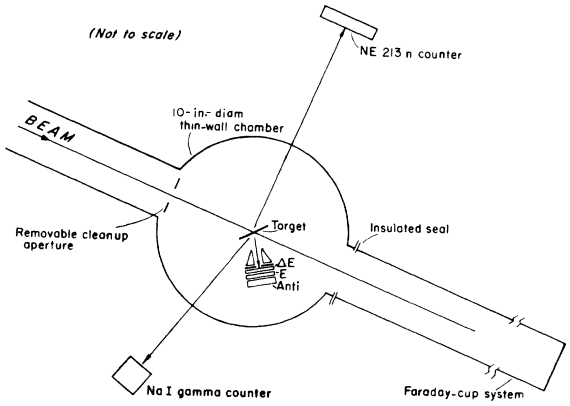

FIG. 2. Arrangement of scattering chamber and detectors.

The γ counter consisted of a 3-in.-by-3-in. NaI crystal placed at about 9 to 12 in. from the target for different runs. Neutrons in the NaI detector accounted for less than 5% of the events in the TOF spectrum, and these were rejected by setting a narrow time window around the prompt γ peak.

A block diagram of the electronic arrangement is shown in Fig. 4, and is referred to below in the description of further details of the counting and analysis system.

Three energy signals, ΔE, E, and E_{anti}, obtained from the charged-particle detector telescope, were amplified, and the E and ΔE amplified signals were sent into analog-to-digital converters (ADC) 1 and 2. In addition, all three amplifier outputs were fed to single-channel analyzers (SCA), the outputs of which were used to establish a ΔE-E-anti coincidence.

The E system generated fast-timing signals which started two time-to-amplitude converters (TAC) used to measure TOF for the neutrons and γ rays. The stop signals were obtained by taking fast signals from the neutron and γ-ray detectors. The TOF spectra from the TAC's were mixed and sent into ADC 3; routing pulses were provided to place the neutron and γ TOF spectra into separate halves of the ADC.

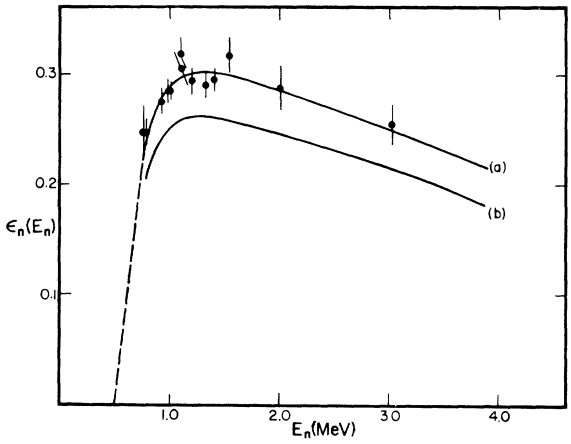

FIG. 3. Efficiency of neutron detector. The experimental points are efficiencies measured at the center of the scintillator, with statistical errors. Curve (a) is an empirical smooth fit through these points. The effective efficiency averaged over the face of the detector, given by curve (b), is 15% lower than the efficiency in (a), due to loss of efficiency near the edge of the detector.

An integrated analog output of the neutron detector was amplified and sent into ADC 6 as a measure of the proton recoil energy (E_{scin}) in the liquid scintillator. PSD against γ rays in the neutron detector was accomplished by measuring the time between a "leading-edge" signal derived from a constant-fraction timing phototube base (CFTPB) and a "crossover" signal generated by a crossover mode SCA fed by a double-delay-line (DDL) amplifier. These signals were used as start and stop inputs for a TAC; the TAC output provided the PSD spectrum sent to ADC 5. The analog signal from the γ detector, after amplification, was sent to ADC 4.

The six ADC's were interfaced to an SDS-930 computer which was used on line to process and store the data. The ΔE and E signals were digitally added, and particle identification was performed using an exponentiation analysis[10] with a lookup table. The remaining ADC signals were only processed to the extent of digital biasing and amplification. Gating of the ADC's was provided by the coincidence between the deuteron system and either the neutron or γ systems. This gating served only to establish a rough time coincidence between events in the detector system. The critical thresholds and windows for selection of accepted events were set using the computer program.

The full array of digitized signals for events satisfying a digital deuteron selection window on the particle-identification spectrum were written event by event on magnetic tape. During on-line analysis or in post-run analysis of the magnetic tapes, those events selected on the basis of further criteria were displayed via an oscilloscope or line printer in the form of one-dimensional or two-dimensional spectra. For neutron-deuteron coincidences, the two-dimensional display was usually of neutron TOF vs deuteron energy, the selection being made by imposing an energy threshold of E_{scin} and a neutron window on the PSD spectrum. For the γ-deuteron coincidences, the two-dimensional display was of NaI scintillator pulse-height vs deuteron energy; the selection was made by imposing a γ window on the TOF spectrum. These two-dimensional displays constituted the basic data of the experiment, while the one-dimen-

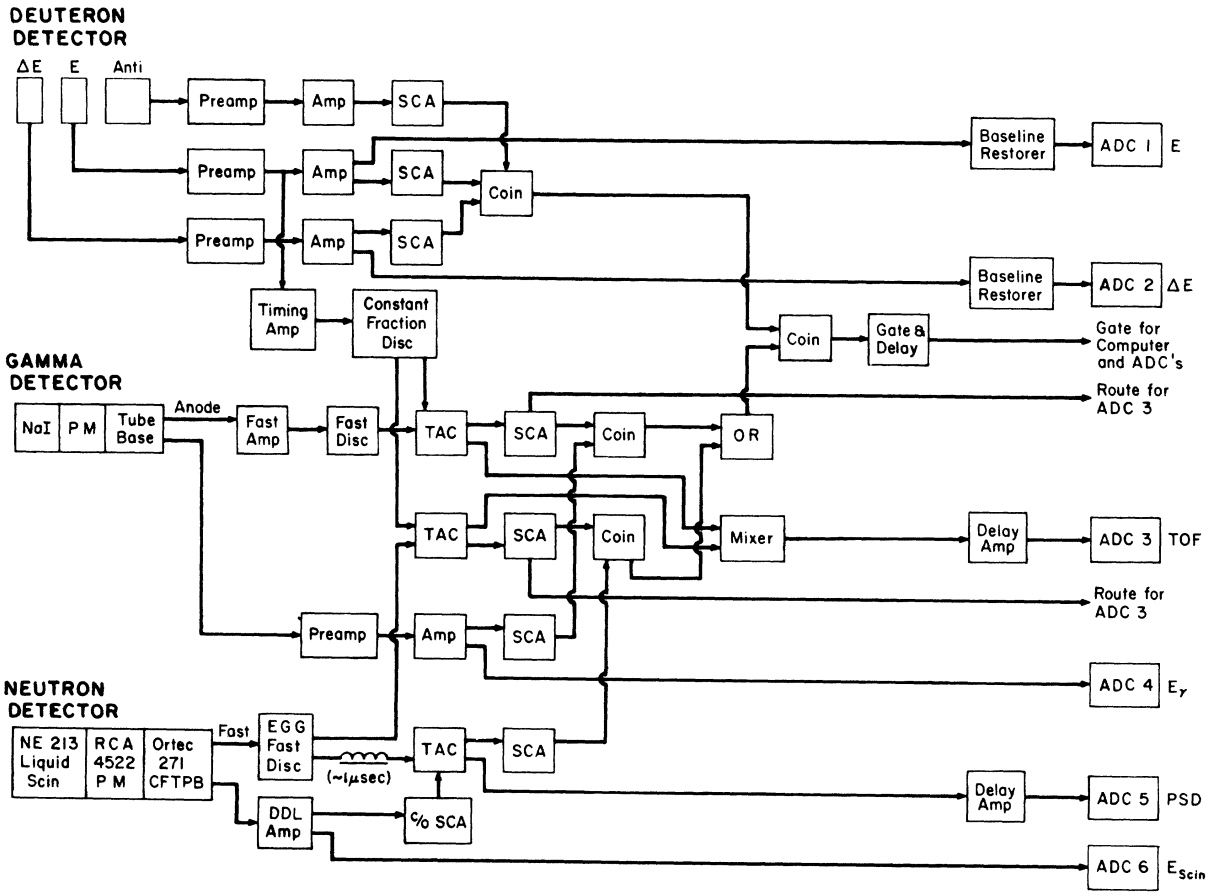

FIG. 4. Schematic block diagram of the electronic arrangement.

sional projected spectra were used for supplementary monitoring purposes.

III. EXPERIMENTAL PROCEDURE FOR FINDING NEUTRON FRACTIONAL YIELDS

A typical two-dimensional display of the data from the ^{61}Ni$(d, d'n)^{60}$Ni reactions is shown in Fig. 5. The events are distributed along curved bands corresponding to kinematic loci for $(d, d'n)$ events leading to the ground state and to excited states of ^{60}Ni. Only the bands for the ground state and first excited state at 1.33 MeV are resolved. On each locus the slowest neutrons are associated with deuterons of highest energy; as the deuteron energy $E_{d'}$ decreases, the ^{61}Ni excitation energy E_i increases, the neutron energy increases, and the flight time decreases correspondingly. As is seen, the ground-state band is dominant only in the region below the threshold for emission to the 1.33-MeV state. Above this threshold, the 1.33-MeV band becomes dominant, depleting the yield to the ground state, and at still higher energies the yield to the 1.33-MeV state becomes depleted by competition with the higher excited states. The horizontal line at the bottom of the figure is due to prompt γ rays; a small fraction of the prompt γ rays were intentionally admitted through the PSD system, in order to facilitate time calibration.

The number of neutron-deuteron coincidence events to the various final states in ^{60}Ni was extracted by summing the counts along the appropriate kinematic band as a function of $E_{d'}$ (or of E_i, equivalently), subtracting background, correcting the net number of counts for the measured neutron-detection efficiency, multiplying by $4\pi/\Delta\Omega$, where $\Delta\Omega$ is the detector solid angle, and inserting a small laboratory-to-center-of-mass kinematic conversion. Background was determined for each value of $E_{d'}$ by sampling the counts in the two-dimensional display in those regions of flight time either too short to contain true events or too long to be associated with neutrons of $E_n > 0.5$ MeV. Sufficient TAC range was used to permit the accumulation of background data during each run. Multiplying by $4\pi/\Delta\Omega$ corrects for the geometric efficiency, under the assumption that the angular distribution of coincident neutrons is isotropic. As discussed in Sec. V, experimental results were obtained which indicate that this is a reasonably good assumption. The kinematic correction was made to translate the results from the laboratory to the ^{61}Ni rest frame, to account for recoil effects accompanying d' emission.

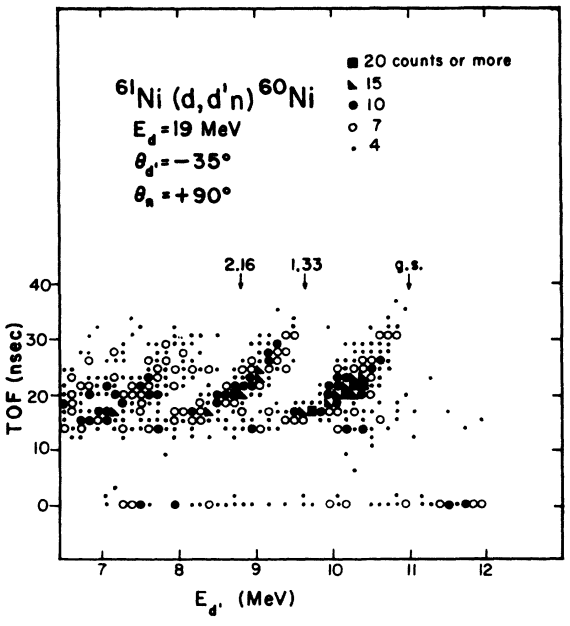

FIG. 5. Neutron TOF vs deuteron energy. The arrows indicate threshold deuteron energies for transitions to the ground state and to low-lying excited states of ^{60}Ni.

At each excitation energy E_i, the neutron fractional yield F_n was extracted by dividing the corrected number of neutron-deuteron coincidence events by the number of inelastically scattered deuterons at the corresponding energy $E_{d'}$. Singles runs to determine the latter quantity were made after each coincidence run, using the same deuteron counter geometry. Relative normalization of the coincidence and single runs was accomplished by comparing scaled counting rates in the deuteron detector. (This is more reliable than using the integrated beam flux, because narrow strip targets were used and some of the incident beam might have missed the target.) Although events from impurities such as ^{12}C and ^{16}O in the target could not contribute to the coincidence yields, they did contribute significantly to the single detector yields, and it was therefore necessary to correct the observed singles spectra on the basis of runs taken with carbon and Mylar targets. Small corrections also were made for isotopic impurities in the targets.

Fractional neutron yields F_n, obtained in the manner outlined above, are shown in Fig. 6 as a function of excitation energy. Again, but more explicitly than in Fig. 5, one sees the successively more important roles of the ground state, the first excited state, and the higher excited states, as the excitation energy increases. The over-all neutron yield increases toward unity, with increasing excitation energy. The comparison of the experimental points to theoretical expectations will be discussed in Sec. V.

The errors shown in Fig. 6 include statistical standard deviations of about 10 to 20% for the coincidence counts, statistical standard deviations of about 5% for the singles counts, uncertainties of about 5% in the background subtraction, and uncertainties of about 5% arising from difficulties in accounting for TOF tails on the kinematic bands. The largest remaining uncertainty arises from the neutron detection efficiency. For the most part, this uncertainty is estimated to be about 10% of the measured efficiency. However, at neutron energies below 1 MeV, where the efficiency varies strongly with energy, the effective uncertainty is increased, because at any point in the bands of Fig. 5 the neutron energy is determined kinematically from the deuteron energy, and small errors in deuteron energy lead to relatively large efficiency errors. For this reason, data below a neutron energy of 0.7 MeV were not used. For excitation energies more than 3 MeV above the ground-state threshold, the neutron yields to all states of ^{60}Ni are summed together, and as the population of the various final states is not known, the efficiency was estimated by using an average efficiency corresponding to an effective average neutron energy of about 1 MeV. An uncertainty of 20% is assigned to this efficiency.

At excitation energies below the threshold for neutron emission to the second excited state of ^{60}Ni, the neutron yield to the first excited state at 1.33 MeV may be measured by observing 1.33-MeV γ rays in coincidence with inelastic deuterons. The 1.33-MeV photopeak stands out reasonably well in the coincidence γ-ray spectra, as seen in Fig. 7. Furthermore, since measured branching ratios[11] indicate that most of the higher excited states decay primarily (over 80%) by cascades through the first excited state, the 1.33-MeV γ ray is a good approximate measure of the total neutron yield to excited states and, at high enough energies for the ground-state yield to be small, of the total neutron yield to all states.

The number of coincidences between inelastic deuterons and the 1.33-MeV γ rays was determined from the coincidence γ-ray spectrum by summing the counts in the 1.33-MeV photopeak as a function of $E_{d'}$, subtracting the continuum background, and dividing by the efficiency-solid-angle factor. This factor was found by measuring the photopeak efficiency for 1.28-MeV γ rays from a calibrated ^{22}Na source, using the same detection geometry as in the actual data runs. This procedure assumes γ-ray isotropy, an assumption which was roughly verified by runs with different γ-ray angles. The normalization procedure for finding fractional yields for the emission of 1.33-MeV γ rays was the same as used for the neutron fractional yields.

A comparison between the neutron yields found from the neutron measurements and the neutron yields found from the 1.33-MeV γ-ray measure-

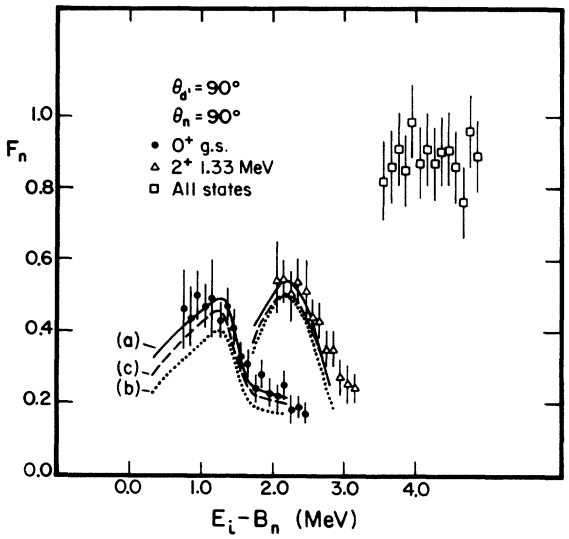

FIG. 6. Experimental and theoretical neutron fractional yields for ^{61}Ni$(d, d'n)^{60}$Ni, as a function of ^{61}Ni residual excitation energy. The group labeled "all" includes the ground state as well as the excited states. The curves are theoretical predictions for: (a) modified spin distribution, $g = 0.5g_R$; (b) modified spin distribution, $g = 0.8g_R$; and (c) unmodified spin distribution, $g = 0.5g_R$ (see text, Sec. V).

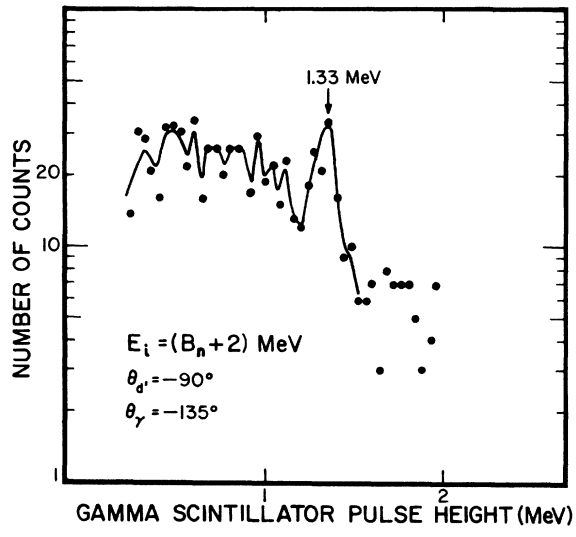

FIG. 7. Pulse-height spectrum in NaI detector for γ rays in coincidence with deuterons. The deuteron energy corresponds to a ^{61}Ni residual excitation energy of $E_i - B_n = 2$ MeV.

ments is shown in Fig. 8. The agreement is quite good. Below the threshold for the second excited state, the yields found by the two techniques are identical. For higher excitation energies the γ-ray results are close to the neutron results, but lie slightly lower. A small difference of this sort is to be expected because the ground-state neutron yield still contributes a small amount, and because the γ cascades are not 100% through the 1.33-MeV state. The 1.33-MeV γ-ray results thus supply a good confirmation of the neutron results; they also provide a measure of F_n for the first excited state at excitation energies for which the neutrons have insufficient energy to be detected themselves.

A further check on the measured neutron fractional yield F_n is possible by determining the fractional γ-ray yield F_γ at excitation energies below the threshold for neutron emission to the first excited state. Although α-particle emission is energetically possible it is here greatly suppressed by the Coulomb barrier, and thus $F_n = 1 - F_\gamma$. F_γ was measured by comparing the coincident γ-ray yields at deuteron energies corresponding to $E_i = B_n$ and $E_i = B_n + 1$ MeV, where $B_n = 7.82$ MeV is the neutron binding energy in ^{61}Ni. The γ-ray pulse-height spectra were observed to have the same shape for the two cases, with mean detected energies of 1.67 and 1.68 MeV, respectively, and thus the detection efficiencies are the same. Assuming the multiplicity of the γ rays for these similar spectra to be proportional to the excitation energy, $F_\gamma(E_i)$ is given by

$$F_\gamma(E_i) = \frac{N_\gamma(E_i)}{N_\gamma(B_n)} \frac{B_n}{E_i} F_\gamma(B_n), \qquad (1)$$

where N_γ is the observed rate for coincident γ rays from ^{61}Ni, normalized to the deuteron singles rate. Note that the γ-ray detection efficiency need not be known. Taking $F_\gamma(B_n) = 1$, it was found for a deuteron angle of 90° that $F_\gamma = 0.61$ at $E_i = B_n + 1$ MeV, implying $F_n = 0.39$, in agreement with the experimental value from the neutron data of $F_n = 0.44 \pm 0.05$.

IV. STUDIES OF INELASTIC DEUTERON SPECTRA

In addition to the poor resolution inelastic deuteron singles spectra measured to normalize the coincidence spectra, runs with better resolution were carried out to study the (d, d') reaction mechanism and to get more detailed information on target impurities. These additional spectra were obtained using a detector system with a smaller angular acceptance to reduce kinematic broadening and with a thickness sufficient to stop all deuterons. The system consisted of a ΔE-E telescope with a 100-μm ΔE detector, a 2000-μm E detector, and a defining aperture subtending an angle of 0.82° in the horizontal plane. The overall resolution was about 80 keV. Large area targets were used instead of the strip targets of the coincidence studies, to permit beam integration for absolute cross-section measurements.

Data were taken for ^{61}Ni from 40 to 160° (lab), and the results for 40, 90, and 160° are shown in Fig. 9. The spectra are dominated by high-energy deuterons at forward angles and by low-energy deuterons at backward angles. Peaks due to ^{12}C and ^{16}O contaminants in the ^{61}Ni target are clearly seen in Fig. 9. To facilitate the subtraction of contaminant contributions in the spectra used for normalization of the coincidence data, the contaminant spectra were also studied with Mylar and carbon targets.

Figure 10 shows the angular distributions of inelastically scattered deuterons, for ^{61}Ni residual excitation energies of 8, 10, and 12 MeV. In general, these angular distributions and the spectral shapes of Fig. 9 indicate the dominance of direct processes in the forward hemisphere. In the backward hemisphere, however, the angular distribu-

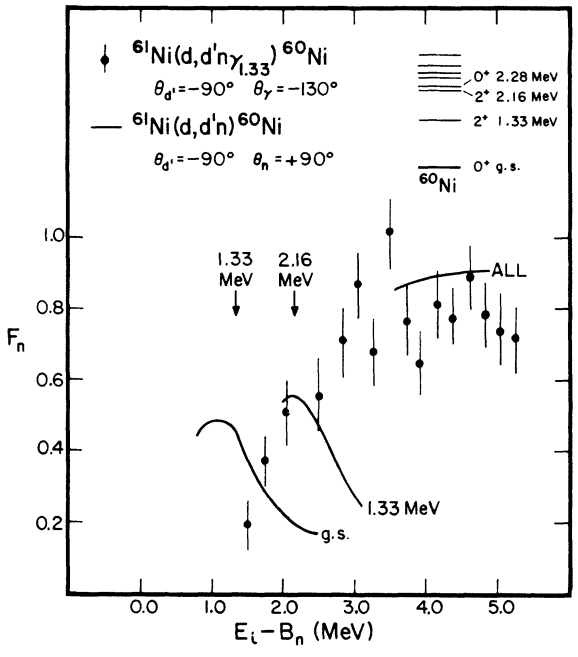

FIG. 8. Comparison of ^{61}Ni$(d, d'n)^{60}$Ni neutron fractional yields from neutron and γ-ray measurements. The curves correspond to empirical smooth fits to the experimental neutron results of Fig. 6. The points are values of F_n extracted from the 1.33-MeV coincident γ-ray yields. The arrows indicate the thresholds for neutron emission to the first and second excited states of ^{60}Ni.

tions tend to become flat, suggesting that the compound-nuclear mechanism plays a significant role, especially for low emitted deuteron energies.

In order to estimate just how much of the spectra are due to compound-nuclear processes, we have computed the theoretical deuteron evaporation spectrum:

$$\frac{d\sigma}{d\Omega}(E_{d'}) = \frac{1}{4\pi}\sigma_{CN}\frac{\Gamma_{d'}}{\Gamma}\frac{\Gamma_{d'}(E_{d'})}{\Gamma_{d'}} . \quad (2)$$

$\sigma_{CN}\Gamma_{d'}/\Gamma$ describes the rate of formation of the compound nucleus ^{63}Cu and its subsequent decay

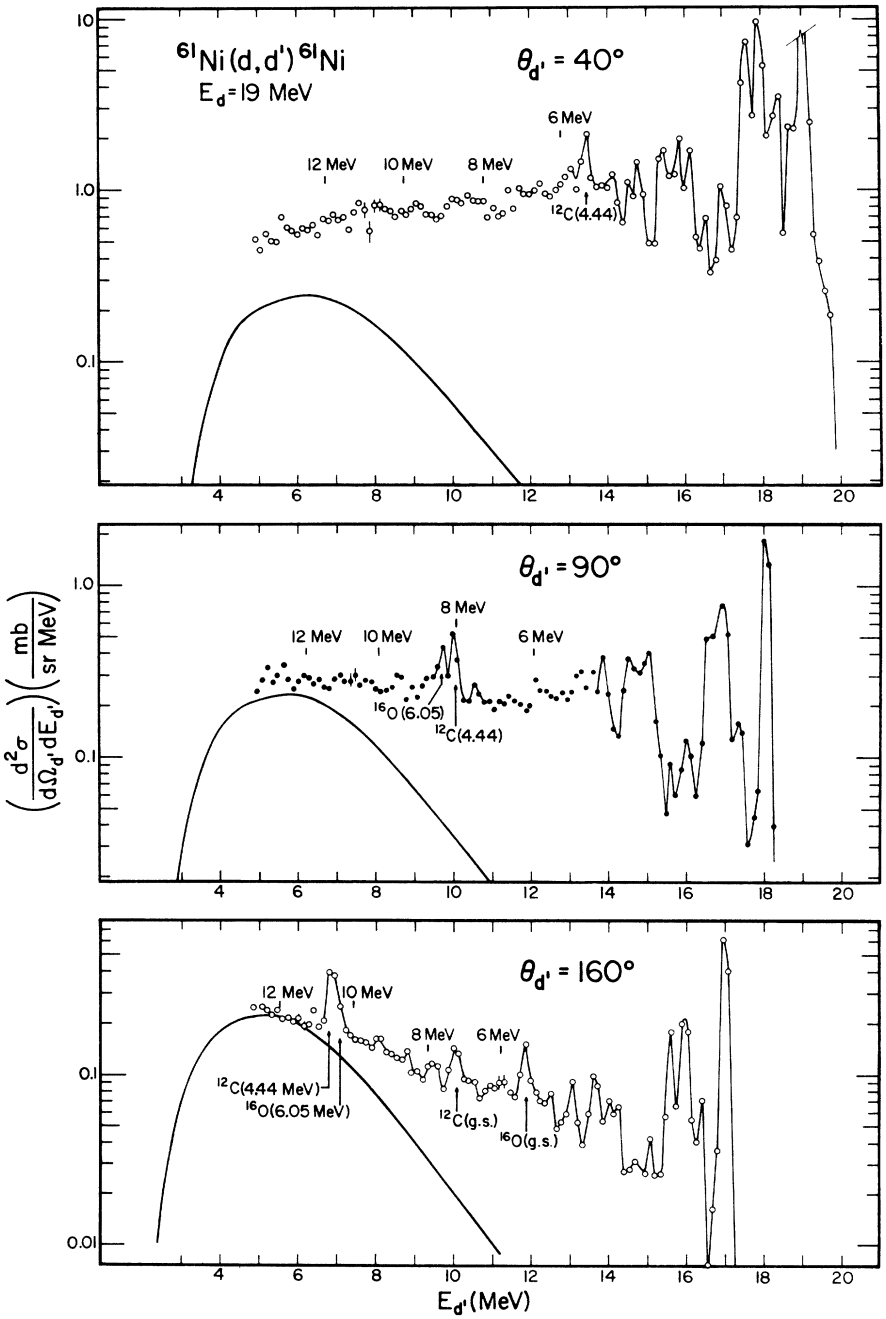

FIG. 9. Energy distributions (lab) for inelastic deuterons from ^{61}Ni. The solid curves are theoretical evaporation spectra (lab), normalized to the 160° experimental cross section. ^{61}Ni residual excitation energies are shown above the experimental points.

into all deuteron channels, and the factor $\Gamma_{d'}(E_{d'})/\Gamma_{d'}$ gives the normalized energy distribution of evaporated deuterons. The angular distribution of these deuterons is taken to be isotropic. Γ_a is the decay width for particle a, and Γ is the total width summed over Γ_a. The widths Γ_a have an energy dependence given by

$$\Gamma_a(E_a)=\frac{2S_a+1}{\pi^2\hbar^2}E_a M_a \sigma_{\text{inv}}(E_a)\rho_f(U_f)/\rho_i(U_i), \quad (3)$$

where S_a and M_a are the spin and reduced mass of particle a, ρ_i and ρ_f are the densities of states in the initial and final nuclei at excitation energies U_i and U_f, and $\sigma_{\text{inv}}(E_a)$ is the cross section for the inverse reaction. The widths $\Gamma_{d'}$ and Γ_n were found by integrating Eq. (3) over the residual energy, using standard spin-independent Fermi-gas level densities.

The total width Γ was calculated as

$$\Gamma=\Gamma_n\left(1+\frac{\Gamma_p}{\Gamma_n}+\frac{\Gamma_\alpha}{\Gamma_n}+\frac{\Gamma_{d'}}{\Gamma_n}\right). \quad (4)$$

Γ_α/Γ_n was assumed to be negligible at the high excitation energies involved in the evaporation from ^{63}Cu. The ratios Γ_a/Γ_n are all small, and were

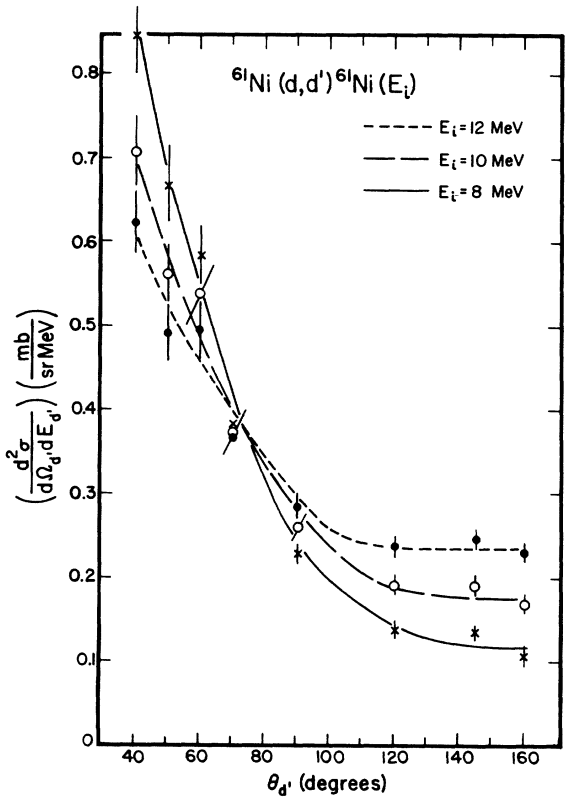

FIG. 10. Angular distributions (lab) for inelastic deuterons from ^{61}Ni, for several residual excitation energies in ^{61}Ni.

calculated using the approximate expression[12]:

$$\frac{\Gamma_a}{\Gamma_n}\cong\frac{(2S_a+1)M_a}{(2S_n+1)M_n}\exp[(B_n'-B_a'+V_n-V_a)/T], \quad (5)$$

where B_n' and B_a' are the separation energies corrected for pairing-energy effects, and V_n and V_a are effective barrier heights; T is the nuclear temperature at the average residual excitation energy. A check of this approximate expression was made by comparing $\Gamma_{d'}/\Gamma_n$ from Eq. (5) and from an interpretation of Eq. (3). The results were 0.0162 and 0.0152, respectively, in satisfactory agreement.

A theoretical absolute normalization of the deuteron spectrum cannot be reliably made because the total compound-nuclear cross section is not known. It is sometimes taken to be the total reaction cross section σ_R given by $\pi\lambda_d^2\sum(2l+1)T_l(E_d)$, but σ_R gives only an upper limit for σ_{CN}, because an unknown fraction of σ_R is depleted by direct processes. Therefore an experimental normalization was used for the theoretical spectra displayed in Fig. 9, matching the calculated spectral shape to the observed spectrum at 160° and at $E_i = 12$ MeV, and taking the evaporation yield to be isotropic. With calculated values $\sigma_R = 1670$ mb and $\Gamma_{d'}/\Gamma = 0.011$, this experimental normalization corresponds to a ratio $\sigma_{CN}/\sigma_R = 0.7$. Results of related studies in neighboring nuclei[13] and general systematics of compound-nuclear reactions indicate that this is a plausible result for 19-MeV deuterons on ^{61}Ni. Thus, within wide uncertainties in the evaporation calculations and in expectations for σ_{CN}/σ_R, the observed low-energy deuteron yield at 160° is consistent with the yield expected from compound-nuclear reactions. A more refined normalization for Fig. 9 would presumably assign some of the low-energy 160° d' yield to direct processes. This was not attempted because there is no good guide to the correct amount of direct yield to introduce, and because the simplified normalization used here is considered adequate for the present purposes of qualitative orientation.

With this normalization, the (d, d') cross section at 160° is 100% compound nuclear for $E_i = 12$ MeV (by definition) and drops to about 35% at $E_i = 8$ MeV. At 90° the compound-nuclear fractions are smaller, being about 80 and 15%, respectively, for the same values of E_i. At forward angles the direct processes account for still more of the reaction cross section, the compound-nuclear fractions at 40° decreasing to about 35 and 5%, respectively. Thus d' emission to states of ^{61}Ni which lie in the relevant energy region (1 MeV $< E_i - B_n <$ 4 MeV) is dominated in the forward direction by direct processes, while at backward

angles there is a large compound-nuclear component.

V. RESULTS AND DISCUSSION

Coincidences between a deuteron and a neutron may arise from: (a) the formation of a compound residual nucleus in a (d, d') reaction, followed by neutron evaporation; (b) the formation of a compound residual nucleus in a (d, n) reaction, followed by deuteron evaporation; or (c) the prompt emission of both the deuteron and neutron, before a compound nucleus is formed. It is a basic premise of the present investigation that (a) is the dominant process. Evidence in support of this contention is presented in the succeeding two paragraphs. It should be emphasized, however, that within the context of (a) there is no necessity that the deuteron itself be the product of an evaporation process. In fact, as discussed in Sec. IV, the initial deuteron is for the most part the product of some form of direct reaction.

Mechanism (b) is very unlikely because deuteron evaporation is much less probable than neutron or proton evaporation in the competition following a (d, n) reaction. A similar argument might be directed against (a). However, in this consideration (a) differs from (b) in two respects: First, (a) is copiously fed by direct (d, d') reactions in which no initial compound nucleus is formed preceding the d' emission; second, if an initial ^{63}Cu compound nucleus is formed, a d-n cascade is much more probable than an n-d cascade. This sort of preference can be understood in terms of the statistical model, if one recognizes that although the deuteron is always unfavored in evaporation the relative deuteron yield will in general be greater at higher nuclear temperatures and therefore at the beginning of the evaporation cascade. However, in the present case, this argument is only of relevance as a qualitative guide, because for the events being studied the cascade terminates in one of the few lowest-lying states of ^{60}Ni and the concept of temperature is inappropriate. Thus, in the second state of a n-d cascade the yield of deuterons is to individual states of ^{60}Ni, in competition with neutron emission to regions of excitation in ^{61}Cu where the level density is roughly 10^4 MeV $^{-1}$. A calculation taking the various competing stages into consideration indicates that the d-n cascade is more probable than the n-d cascade by a factor of more than 100. In conjunction with consideration of the noncompound (d, d') events, this confirms that the use of deuterons eliminates the ambiguity as to which particle comes first in the evaporation cascade.

The argument against (c) is based on the angular distributions of neutrons observed in coincidence with deuterons, obtained with the deuteron detector angle fixed. Plots are shown in Fig. 11 of F_n as a function of neutron angle, with the deuteron detector at 90°, for several different excitation energies of ^{61}Ni and final states of ^{60}Ni. In each case the neutron yield is roughly symmetric about 90°, with a slight minimum at 90°. Results similar to those of Fig. 11 were obtained in runs with the deuteron detector fixed at 30°, where again neutrons in the forward and backward direction were found to have equal yields. This type of angular distribution (with a small shift from the 90° symmetry due to the prior d' emission) is characteristic of statistical-model evaporation. On the other hand, were the neutron emitted together with the deuteron one would expect forward neutron peaking, or possibly a strong neutron angular correlation in the direction of the outgoing deuteron. The absence of a significant correlation between the deuteron and neutron directions was demonstrated by comparing neutron yields

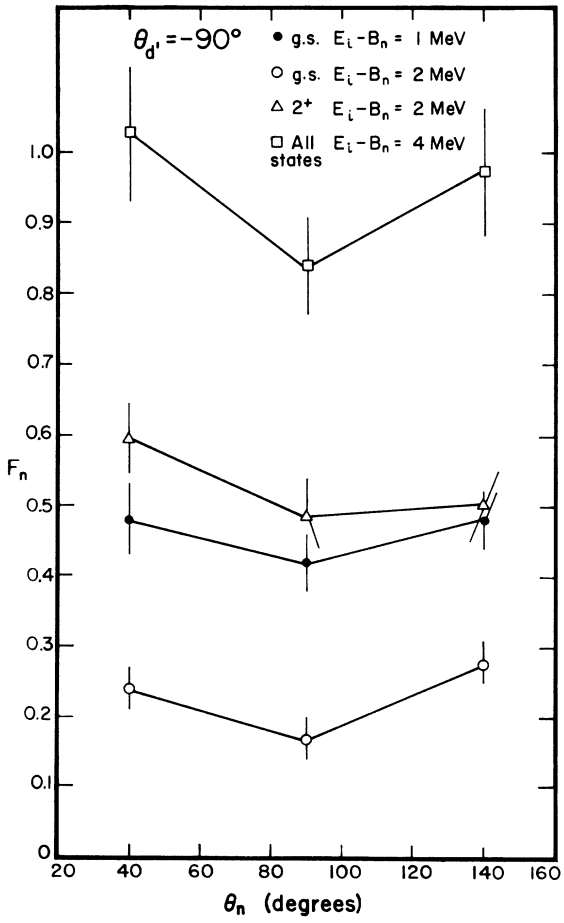

FIG. 11. ^{61}Ni$(d, d'n)^{60}$Ni neutron fractional yields as a function of neutron angle, for fixed deuteron angle.

with both detectors on the same side of the incident beam to yields obtained using the normal geometry. With the neutron detector fixed at +90°, the neutron yields were the same for the deuteron detector at +40 and at −40°.

In view of this evidence against the importance of mechanisms (b) and (c), and the consistency between the observed neutron angular distributions and the expectations for (a), it is concluded that (a) is the dominant reaction mechanism. As seen from the inelastic deuteron spectra of Sec. IV, direct (d, d') reactions are responsible for the bulk of the coincidence events at forward deuteron angles, while evaporation from the ^{63}Cu compound nucleus is more important for backward deuteron angles. Comparisons of the fractional neutron yields F_n at different deuteron angles are displayed in Figs. 12 and 13. From the several displays of Fig. 12, it can be seen that the neutron yields to the ground state and first excited state are rather independent of angle. The same result is exhibited more explicitly in the curves of Fig. 13. In view of the differences in the magnitudes of the direct and compound-nuclear contributions at different deuteron angles, these results indicate that the relative neutron-γ yields are roughly the same for the two mechanisms, at least when the ^{61}Ni nucleus is left at excitation energies not too far above the neutron binding energy. At higher excitation energies, on the other hand, Figs. 12 and 13 show a pronounced dip in neutron yield for forward deuteron angles. This is a puzzling result and will be discussed separately below. For the moment we will concentrate on the implications of the similarity at lower excitation energies.

The most obvious consequence of this observed similarity is the encouragement it gives to the calculation of the expected magnitudes of F_n on the basis of the statistical model for compound-nuclear reactions. This model, aside from uncertainties in parameters, gives a definite formalism for predicting the relative neutron and γ-ray yields. No similarly clear prescription is provided by a direct-interaction model for the (d, d') reaction, because of the difficulty of calculating the spin distribution of the intermediate nucleus.

We turn then to the calculation of F_n in the context of the statistical model. Details of this calculation are presented in the Appendix. The calculation involves two steps: the determination of the spin-parity distribution $P_i(J_i, \pi_i, E_i)$ of the excited ^{61}Ni nucleus as a function of its excitation energy E_i, and the determination of the neutron and γ-ray widths for decay from states of given spin and excitation energy. The fractional neutron yield to a final state of ^{60}Ni of spin-parity (J_f, π_f) and excitation energy E_f is then

$$F_n(E_i, E_f, J_f, \pi_f) = \sum_{J_i, \pi_i} P_i(J_i, \pi_i, E_i) \times f_n(E_i, J_i, \pi_i, E_f, J_f, \pi_f), \quad (6)$$

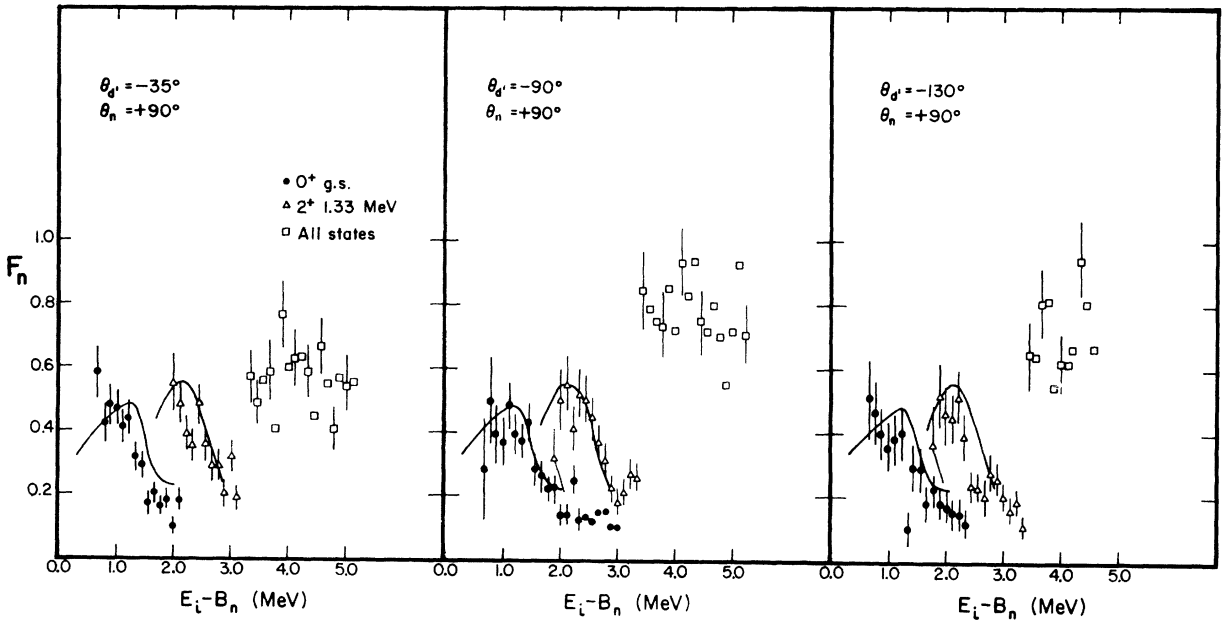

FIG. 12. ^{61}Ni$(d, d'n)^{60}$Ni neutron fractional yields as a function of ^{61}Ni residual excitation energy, for several deuteron angles. The solid lines are the theoretical curves (a) of Fig. 6.

where $f_n(E_i, J_i, \pi_i, E_f, J_f, \pi_f)$ is the ratio of the neutron width to state (E_f, J_f, π_f) to the total width for the decay of the state (E_i, J_i, π_i). The total width is assumed to comprise only neutron and γ-ray channels because charged-particle emission is strongly inhibited by the Coulomb barrier, the binding energies for neutrons, protons, and α particles being $B_n = 7.82$ MeV, $B_p = 9.86$ MeV, and $B_\alpha = 6.47$ MeV. In the energy region under consideration, $0 < E_i - B_n < 4$ MeV, the maximum proton energy is 2.0 MeV and the maximum α-particle energy is 5.4 MeV, both well below the respective Coulomb barriers.

The spin distribution of the ^{61}Ni is calculated by determining the spin distribution of the ^{63}Cu nuclei formed by the incident deuterons, and then the redistribution attendant upon deuteron evaporation. The redistribution involves the angular momentum dependence of the ^{61}Ni level density, which is commonly parametrized in terms of the nuclear moment of inertia $\mathcal{I}$. Recent measurements and summaries[14] suggest that at E_i near 10 MeV, for a nuclear radius parameter r_0 of 1.2 F, the level density can be described using a moment of inertia between about $0.4\,\mathcal{I}_R$ and $1.0\,\mathcal{I}_R$, where $\mathcal{I}_R$ is the nominal rigid-body moment of inertia. The present calculations have been made primarily with $\mathcal{I} = 0.5\,\mathcal{I}_R$ and $\mathcal{I} = 0.8\,\mathcal{I}_R$.

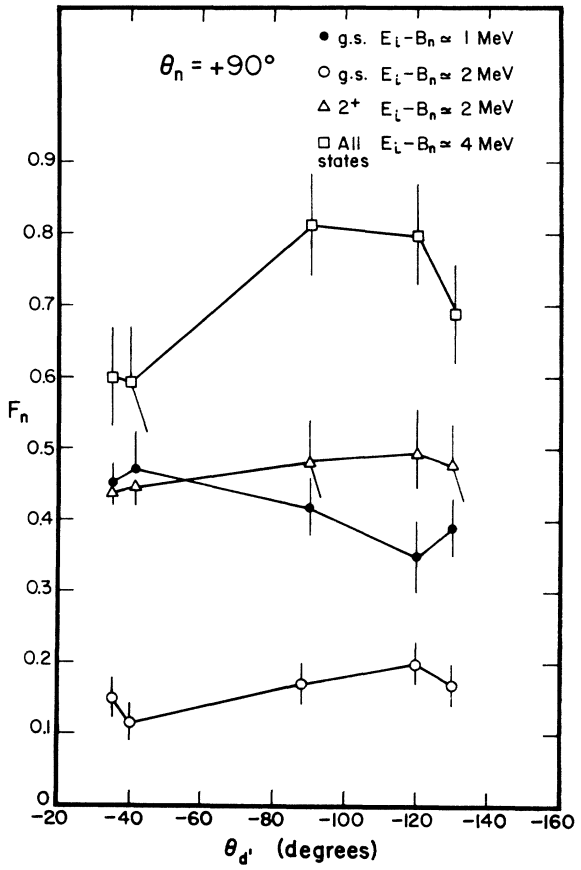

FIG. 13. ^{61}Ni$(d, d'n)^{60}$Ni neutron fractional yields as a function of deuteron angle, for fixed neutron angle.

In calculating the γ-ray-emission width it was assumed that the γ-ray emission was predominantly dipole. The ratio of final-to-initial level density will then be only weakly dependent on spin, and in consequence the spin dependence of the γ width is ignored. The neutron widths, on the other hand, are very strongly spin-dependent because the neutrons are constrained to go to a small number of discrete states of ^{60}Ni. For the 0^+ ground state, this usually requires a large change in spin angular momentum and therefore a high orbital angular momentum l for the neutron. For the 2^+ state a similar, but less extreme, condition exists. The strong l dependence of the neutron transmission coefficients, again obtained from optical-model calculations, produces a very strong dependence of neutron width on initial spin. The dependence is so strong, in fact, that for most initial spin states there is an all-or-nothing situation in which emission is either almost entirely by neutrons or almost entirely by γ rays. Competition between these modes usually exists for only one or two intermediate spin values, as seen in Fig. 14. Thus the values of F_n are to a large extent a reflection of the spin population of ^{61}Ni, and the measurement of F_n is not a sensitive way of experimentally verifying calculated neutron and γ-ray widths. (For example, changing the γ width by a factor of 2 produces only a 10% change in the peak magnitude of the ground-state neutron yield.) Conversely errors in these widths do not have a large effect on the calculated results. On the other hand, F_n is very sensitive to the spin distribution; a translation of the distribution by one unit $\hbar$ decreases F_n by about 30% at the ground-state peak.

As yet, no consideration has been given to the possible role of stripping and other direct reactions in altering the ^{61}Ni spin distribution. These are presumably largely surface reactions, and as such deplete deuterons with high orbital angular momentum, leading to a lower mean spin for the ^{63}Cu compound nuclei than the value predicted by a pure statistical-model calculation. To explore the consequences of this sort of depletion, the ^{63}Cu spin distribution has been calculated in both the normal fashion and with the omission of the 20% of the ^{63}Cu formation cross section with the highest values of l. These distributions will be termed the unmodified and modified spin distributions, respectively, in future reference. The mean values of the corresponding ^{61}Ni spin distributions at $E_i = 8.1$ MeV and with $\mathcal{I} = 0.5\,\mathcal{I}_R$, are

$3.96\hbar$ and $3.60\hbar$, respectively.

Experimental measurements of F_n, with both detectors at 90°, are presented in Fig. 6, together with several theoretical curves representing the calculational options mentioned above. The experimental points and the theoretical curves exhibit certain basic qualitative features of the $(d, d'n)$ reaction. Below the threshold for decay to the first excited state, neutron decay to the ground state rises steadily with increasing excitation energy, but the ground-state fractional yield never rises above 0.5, because, even at $E_i - B_n = 1.33$ MeV, γ emission wins out in the decay of higher-spin states of ^{61}Ni. As neutron decay (at first unobserved in the neutron data) to the 1.33-MeV state becomes energetically possible the neutron yield to the ground state begins to fall off. At still higher excitation energies, in turn, the yield to the first excited state falls off as decay to higher excited states becomes possible. Neutron groups to these higher states were not experimentally resolved, and therefore above $E_i - B_n = 3.0$ MeV the yields to all states, including the ground state and first excited state, were summed together, and an estimated average neutron detection efficiency was used.

The three theoretical curves plotted in Fig. 6 explore the use of the unmodified and modified spin distributions and moments of inertia of $0.5\,\vartheta_R$ and $0.8\,\vartheta_R$. It is seen that the closest match to the experimental points for the neutron yields to the ground and first excited states is obtained for the modified spin distribution and for $\vartheta = 0.5\,\vartheta_R$. This curve is therefore adopted as the "standard" theoretical curve and is the curve employed in other figures for orientation purposes. In noting the rather good agreement between the standard curve and the experimental points for the ground and 1.33-MeV states it is not suggested that either the modified spin distribution or the parametrization leading to $\vartheta = 0.5\,\vartheta_R$ represent "best fits." They merely represent reasonable assumptions which, taken together, lead to a satisfactory reproduction of the data, within the rather large experimental uncertainties.

For the data above $E_i - B_n = 3.0$ MeV the calcu-

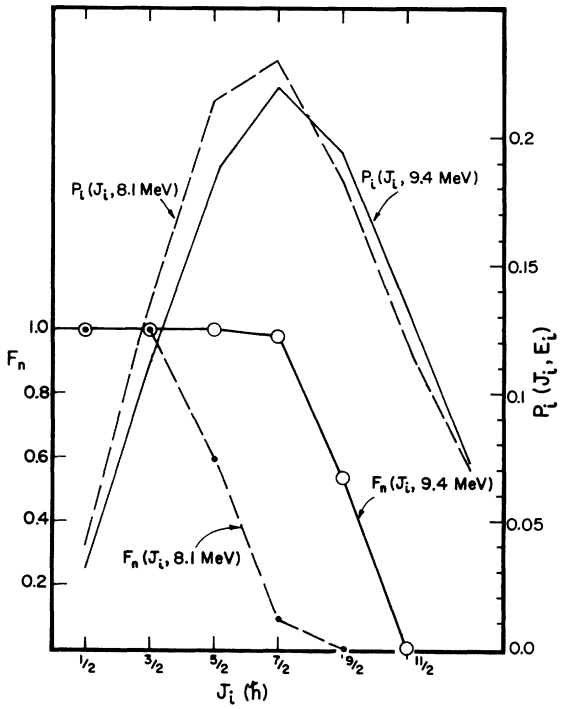

FIG. 14. Theoretical ^{61}Ni$(d, d'n)^{60}$Ni neutron fractional yields $F_n(J_i, E_i)$ as a function of ^{61}Ni spin at two ^{61}Ni residual excitation energies, and calculated spin populations $P_i(J_i, E_i)$ of ^{61}Ni at the same excitation energies. The spin populations were calculated for 19-MeV incident deuterons, using the modified spin distribution and $\vartheta = 0.5\vartheta_R$. The calculated values of F_n are an average over equally populated positive- and negative-parity states.

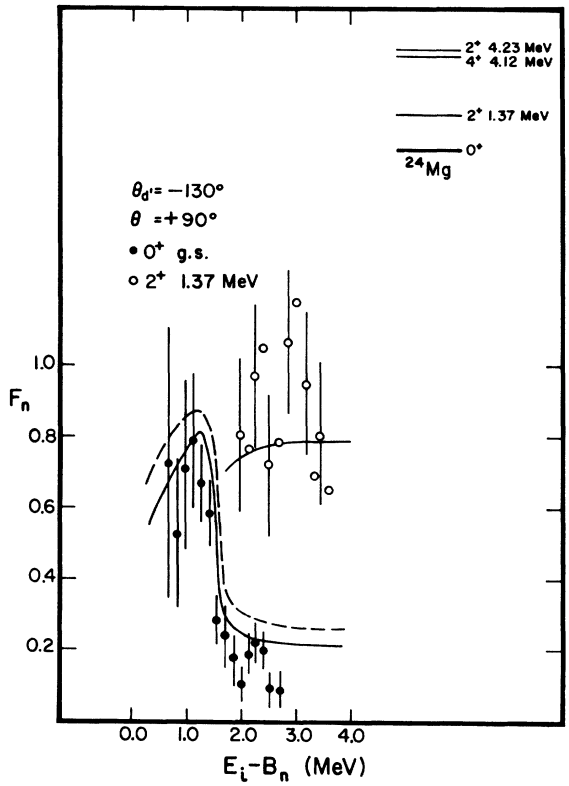

FIG. 15. Experimental and theoretical neutron fractional yields for ^{25}Mg$(d, d'n)^{24}$Mg as a function of ^{25}Mg residual excitation energy. The theoretical yields are calculated for the unmodified spin distribution and $\vartheta = \vartheta_R$.

lated curve for any parametrization rises rapidly to $F_n = 1.0$, as the available neutron energy rises and more states become open to neutron decay. However, the experimental points cluster around $F_n = 0.9$. This discrepancy is not considered to be significant, in view of the uncertainties in the neutron detection efficiency for this group. However, it may in part be a manifestation of a weak minimum in the neutron angular distribution at $\theta_n = 90°$ (see Fig. 11).

Despite the good agreement between observations and expectations in most of the ^{61}Ni data, there is the puzzling anomaly mentioned earlier for $E_i - B_n > 3$ MeV at forward deuteron angles. Here, as was seen in Figs. 12 and 13, F_n is much lower for $\theta_{d'} = 30$ or 40° than for $\theta_{d'} = 90°$. The neutron data for $E_i - B_n > 3$ MeV are of relatively poor quality, because they involve unresolved transitions to a mixture of states, and the neutron energies and detection efficiencies can only be estimated roughly. However, although an overestimate of the efficiency could lead to an underestimate of F_n, it is very difficult to see how it could lead to a dependence of F_n on deuteron angle, even allowing for small shifts in the neutron energy spectrum due to kinematic recoil effects. Further evidence in support of the validity of the low F_n data comes from the 1.33-MeV γ yields, which give values of F_n in agreement with the neutron measurements.

The low value of F_n could, in principle, arise from an overestimate of the deuteron yield. In fact, an error of this sort occurred in the initial data at forward deuteron angles, caused by stray beam entering the detector system directly, without scattering from the target.[15] This difficulty was corrected for the final runs which constitute the results reported here. Similarly, studies of ^{12}C and ^{16}O impurity contributions indicate that it is unlikely that they could cause an error of more than 15%, which is hardly enough to explain the magnitude of the anomaly. Thus the anomalously low value of F_n cannot be dismissed on the ground of experimental uncertainties.

On the other hand, if $F_n \sim 0.6$ at $E_i - B_n > 3$ MeV, it is difficult to account for the remaining decay of the excited ^{61}Ni. With many states available for neutron emission, γ decay should not be of importance. α-particle decay, although energetically allowed, is also expected to be small. For example, for 6-MeV α particles, corresponding to

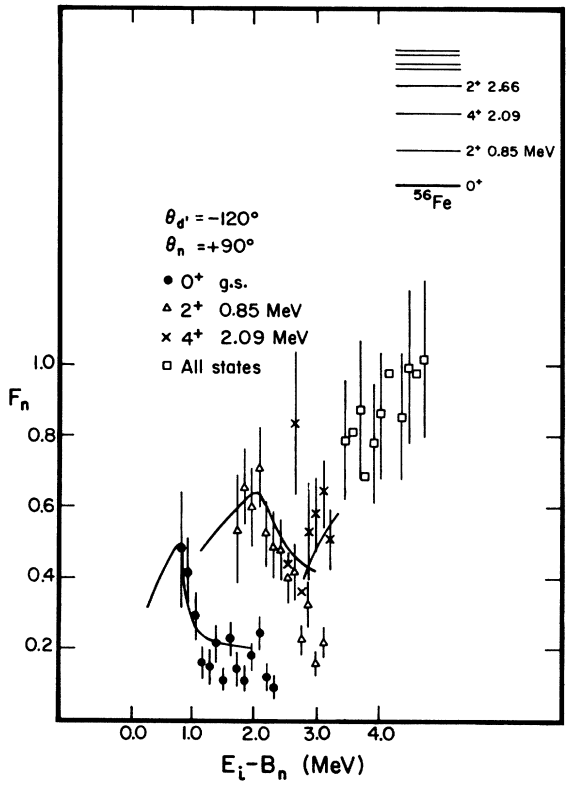

FIG. 16. Experimental and theoretical neutron fractional yields for ^{57}Fe$(d, d'n)^{56}$Fe as a function of ^{57}Fe residual excitation energy. The theoretical yields are calculated for the modified spin distribution and $g = 0.5g_R$.

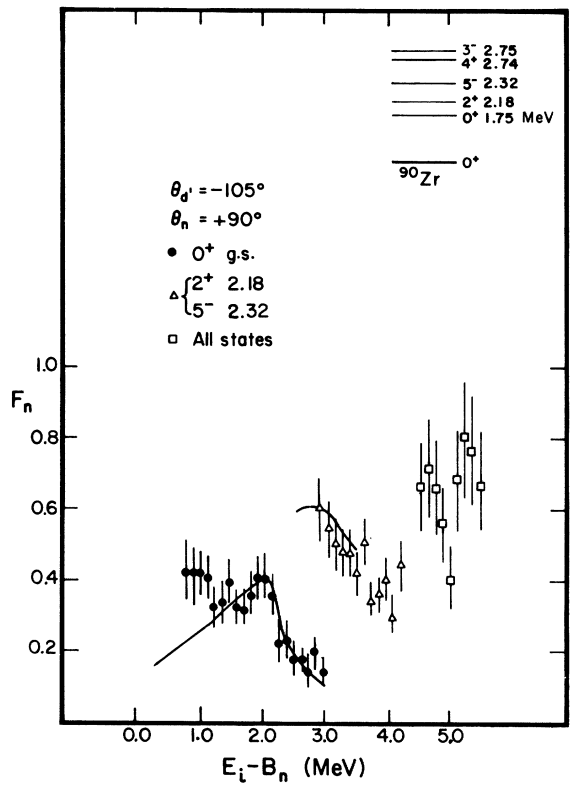

FIG. 17. Experimental and theoretical neutron fractional yields for ^{91}Zr$(d, d'n)^{90}$Zr as a function of ^{91}Zr residual excitation energy. The theoretical yields are calculated for the modified spin distribution and $g = 0.5g_R$.

$E_i - B_n = 4.65$ MeV, the $l=0$ transmission coefficient is about 2×10^{-3}, which is much less than the transmission coefficients for neutrons with $E \geq 1$ MeV and $l \leq 2$ or $E \geq 2$ MeV and $l \leq 4$. Conceivably some other process might contribute, such as forward-peaked production of excited ^{6}Li*, followed by its breakup. Similarly, $(d, {}^3\text{He}^*)$ or $(d, {}^3\text{H}^*)$ could, in principle, also contribute to this anomaly, although there are no well-established states of ^{3}He or ^{3}H in this region.[16] The near isotropy of the coincident neutron yield, including yields in test runs with the deuteron and neutron detectors on the same side of the beam, does not support the ^{3}H* hypothesis. No adequate search was made for deuteron-proton or deuteron-α-particle coincidences, so that neither the ^{3}He* nor ^{6}Li* hypotheses nor some unexpected alternative mechanism for producing protons or α particles can be excluded on purely experimental grounds. However, the observational evidence against ^{3}H* can be interpreted as evidence against ^{3}He* as well, and there is a substantial barrier against ^{6}Li emission. We hesitate, therefore, to place very much hope in such mechanisms being quantitatively adequate to explain the anomaly. For the moment, the matter presents an unsolved puzzle. It is interesting to note that a similar anomaly was reported by Cohen *et al.*[7] in their $(p, p'n)$ investigations with ^{61}Ni. Again the yield to the higher states was inexplicably low, although the data reported were with both detectors at 90°, and thus did not particularly involve forward-peaked events.

Neutron measurements similar to those made for ^{61}Ni were also made for ^{25}Mg, ^{57}Fe, ^{91}Zr, and ^{119}Sn, again for 19-MeV incident deuterons, although for the most part at only one pair of angles. Results of these measurements are shown in Figs. 15 through 18, together with calculated values of F_n. As seen in these figures, the observed and calculated magnitudes of F_n are in rough qualitative agreement.

However, appreciable difficulties exist. To obtain the degree of agreement achieved for ^{25}Mg, it was necessary to use $g = g_R$ and drop any correction for the loss to stripping reactions of high angular momentum components of the incident beam. Retaining the same assumptions as used in the ^{61}Ni analysis, namely $g = 0.5 g_R$ and modifying the spin distribution with a 20% correction for stripping, gives poor agreement. The ^{61}Ni prescription was used with reasonable success for the remaining nuclei, although a somewhat lower moment of inertia would have improved the ^{119}Sn fit. The uncertainties due to target impurities were particularly severe for the ^{25}Mg and ^{119}Sn targets, and therefore it would be premature to interpret these results as evidence for a dependence on mass number of g/g_R or of the stripping contribution. As far as other anomalies in the data are concerned, the low value of F_n at high excitation energies for ^{91}Zr and ^{119}Sn could be due to a high yield of low-energy neutrons to higher excited states in ^{90}Zr and ^{118}Sn, but the high F_n for 1-MeV neutrons to the ground state of ^{90}Zr is a surprising unexplained effect.

Despite these anomalies, there are impressive consistencies in the results. Ground-state neutron yields decrease with increasing mass number, because at higher A the neutron must compete with γ rays going to regions of higher level density and because the spin distribution of the intermediate nucleus is weighted toward higher spins. Furthermore, the relative neutron yields to individual states of the final nucleus can be explained in terms of the specific level structure of the nucleus involved. Thus the yield to the first excited state of ^{24}Mg remains large up to relatively high excitation energies because of the large distance to the second excited state. Particularly good agreement is found for ^{57}Fe, where the calculation reproduces the main features of the com-

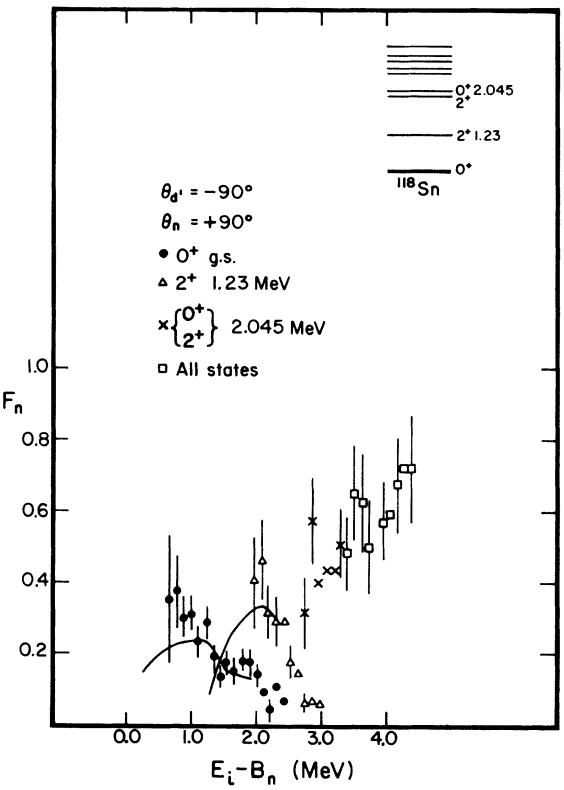

FIG. 18. Experimental and theoretical neutron fractional yields for ^{119}Sn$(d, d'n)^{118}$Sn as a function of ^{119}Sn residual excitation energy. The theoretical yields are calculated for the modified spin distribution and $g = 0.5 g_R$.

petition between γ emission and neutron emission to the ground state, the relatively low-lying 2^+ first excited state, and the 4^+ second excited state.

VI. SUMMARY AND CONCLUSIONS

The most immediate implication of the present results is the strong evidence yielded for the importance of γ-ray competition in nuclear evaporation processes, even when the available energy for neutron emission is as high as 1 or 2 MeV and the incident projectile is relatively light. These results can be understood in terms of the spin population of the intermediate compound nucleus, and are a consequence of the rapid decrease in neutron transmission coefficients with increasing l. The conclusion that an intermediate compound nucleus is formed in the $(d, d'n)$ reaction is based largely on the observed near isotropy of the coincident neutron yield for fixed deuteron angle.

A quantitative explanation of the magnitude of the fractional neutron yields is given by the statistical model. Rather extensive agreement between observed and calculated yields was obtained on the basis of this model, especially for the target most studied, ^{61}Ni. The agreement is in part attributable to choices made for the moments of inertia and for corrections to the spin distribution. However, these choices agree reasonably with *a priori* expectations, and thus are consistent with the over-all description.

The extent of the agreement with statistical-model calculations is surprising. The statistical model might be expected to predict correctly relative neutron and γ-ray yields from compound nuclei of given spin and excitation energy. However, it is not apparent why the spin distribution itself should be successfully predicted, especially as the measured (d, d') angular distributions, spectra, and yields show that the emitted deuterons are predominantly direct at forward angles, with a compound-nuclear component which becomes important only at backward angles. Despite this difference in the nature of the (d, d') process, the neutron fractional yields were found to be independent of deuteron angle for $E_i - B_n < 3$ MeV. This implies that the ^{61}Ni residual nuclei have the same spin distribution for different deuteron-emission angles, and thus the spin distribution shows no strong dependence on angle for direct (d, d') reactions or on whether the (d, d') process is direct or compound nuclear. As suggested by Cohen *et al.*,[7] a similarity between direct and compound-nuclear spin distributions can be qualitatively understood if for direct reactions the average impact parameter is higher and the average fractional angular momentum transfer is lower than for compound-nuclear reactions. It is nevertheless surprising that the similarity is as close as it was found to be, especially in view of the sensitivity of the neutron yield to spin.

In spite of the over-all agreement with statistical-model calculations, there still exist several discrepancies. The most striking of these is the apparent dependence on deuteron angle of the neutron fractional yield for relatively highly excited states of ^{61}Ni. Conceivably, this anomaly is attributable to neglected charged-particle competition, but at present this explanation is purely conjectural.

ACKNOWLEDGMENTS

We are grateful to D. D. Chamberlin and D. L. Oberg for their invaluable assistance in the many experimental runs. It is a pleasure to thank Professor R. Vandenbosch for his continued interest in this investigation and for many helpful suggestions. Helpful comments from Professor I. Halpern and his critical reading of the manuscript are also gratefully acknowledged. The assistance of D. R. Brown and G. Liu during the final phases of the experiments is appreciated. One of us (C.L.) wishes to thank the staff and students at the Nuclear Physics Laboratory, University of Washington, for their kindness and help throughout his graduate studies.

APPENDIX

The neutron fractional yield has been calculated using the standard techniques of the compound-nuclear statistical model.[17] In this formalism the fractional probability for neutron emission from states CN_i of a compound nucleus at excitation energy E_i to a final state of excitation energy E_f and spin and parity (J_f, π_f) is

$$F_n(E_i, E_f, J_f, \pi_f) = \sum_{J_i, \pi_i} P_i(J_i, \pi_i, E_i) \times f_n(E_i, J_i, \pi_i, E_f, J_f, \pi_f), \tag{A1}$$

where $f_n(E_i, J_i, \pi_i, E_f, J_f, \pi_f)$ is the ratio of the neutron decay width to the state (E_f, J_f, π_f) to the total decay width of states (E_i, J_i, π_i), and $P_i(J_i, \pi_i, E_i)$ is the fractional spin-parity distribution for CN_i.

A. Level Densities

The evaluation of level densities for the present analysis follows largely the formulation of Gilbert and Cameron.[18] For excitation energies above a dividing point (which varies from nucleus to nucleus, and which is typically about 5 MeV near $A = 60$) they use a nuclear level density of the Fermi-gas

form:

$$\rho(U,J)=\frac{2J+1}{2\sqrt{2\pi}\sigma^3}\exp\left[-\frac{(J+\frac{1}{2})^2}{2\sigma^2}\right]\left(\frac{\sqrt{\pi}}{12}\,\frac{e^{2\sqrt{aU}}}{a^{1/4}U^{5/4}}\right). \tag{A2}$$

For energies below this point, a spin-independent form is used:

$$\rho(E)=(1/T)e^{(U-E_0)/T}. \tag{A3}$$

In these expressions E is the excitation energy of the nucleus, and U is the excitation energy corrected by the subtraction of the pairing energy. T is the nuclear temperature; a is the conventional level-density parameter, with shell corrections included; and E_0 is a normalization parameter for Eq. (A3). For the analyses of this paper, values of the pairing energies, T, and a are taken from the tabulations of Gilbert and Cameron. In some parts of the present analysis a hybrid level-density expression is employed:

$$\rho(U,J)\propto\frac{2J+1}{\sigma^3}\exp\left[-\frac{(J+\frac{1}{2})^2}{2\sigma^2}\right]e^{U/T}. \tag{A4}$$

The spin dependence of the level density is described in Eqs. (A2) and (A4) in terms of the spin cutoff parameter σ^2. In the analysis below, σ^2 is evaluated through an equivalent parametrization in terms of the nuclear moment of inertia $\mathcal{I}$, which is related to σ^2 by the relation $\sigma^2=\mathcal{I}t/\hbar^2$, where t is the thermodynamic temperature given by $U=at^2-t$. The moment of inertia was expressed in terms of the nominal rigid-body value $\mathcal{I}_R$ by the relation $\mathcal{I}=K\mathcal{I}_R$, where $\mathcal{I}_R=\frac{2}{5}MAR^2$, M is the nucleon mass, A is the mass number, and $R=r_0A^{1/3}$ with $r_0=1.2$ F.

B. Calculation of the Distribution $P(J_i, \pi_i, E_i)$

The spin-parity distribution of the compound system CN_i formed after d' evaporation from the original compound nucleus CN_0 is given by

$$P_i(J_i,\pi_i,E_i)=\frac{1}{2}\sum_{J_0}P_0(J_0)\frac{\rho(U_i,J_i)T(J_0,E_{d'},J_i)}{\sum_J\rho(U_i,J)T(J_0,E_{d'},J)}. \tag{A5}$$

Here $P_0(J_0)$ is the spin distribution of CN_0 and is found from the relation

$$P_0(J_0)=\frac{(2J_0+1)T(J_t,E_d,J_0)}{\sum_J(2J+1)T(J_t,E_d,J)}. \tag{A6}$$

The transmission factor $T(J_t,E_d,J_0)$ is defined as

$$T(J_t,E_d,J_0)=\sum_{S=|J_t-s|}^{J_t+s}\ \sum_{l=|J_0-S|}^{J_0+S}T_l(E_d), \tag{A7}$$

where s, J_t, and J_0 are the spins of the deuteron, target, and CN_0, respectively, and $T_l(E_d)$ is the transmission coefficient for the incident deuteron of energy E_d and orbital angular momentum l. $T(J_0,E_{d'},J_i)$ is the corresponding summation for d'. The ratio of level densities in Eq. (A5) was evaluated using the spin-dependent part of Eq. (A2).

The factor $\frac{1}{2}$ in Eq. (A5) arises from the demands of parity conservation. Assuming that the transmission coefficients are approximately the same for neighboring l, which holds true for the incident 19-MeV deuterons, CN_0 will be formed with roughly equal probability in states of positive and negative parity. On the reasonable assumption that the level densities for states of different parity are approximately equal,[19] states of either parity will also be formed with approximately equal probabilities in CN_i. However, in view of the parity restrictions in the decay of CN_i to low-lying final states, it is necessary to consider the parities of CN_i in calculating decay widths, and thus half the spin distribution is explicitly assigned to states of each parity. [The same factor $\frac{1}{2}$ is obtained if one explicitly includes parity conservation in the specification of ρ and T in Eq. (A5) and sums over parity in the denominator.]

The transmission coefficients used in the calculation of $P_i(J_i,\pi_i,E_i)$ were obtained using an optical-model code with a conventional Woods-Saxon potential. The parameters used for this potential were taken from Perey and Perey.[20]

Although the present calculation is made on the supposition that a compound nucleus is formed in the first stage of the reaction, it is recognized that there is important competition from direct stripping and inelastic events. These direct reactions tend to be localized at the nuclear surface and thus take place with large values of angular momentum. To explore the effects of the direct reactions, 20% of the (unmodified) distribution $P_0(J_0)$ was removed from the high-angular-momentum region for some of the calculations (i.e., for the "modified" spin distribution) and the truncated distribution renormalized to 100%.

C. γ Widths

In the calculation of γ-ray widths, we have assumed that γ-ray emission is predominantly electric dipole. Two approaches were used in the calculating the widths, both recently discussed by Lynn.[21]

The first approach is based on a calculation of the radiation width in a simplified single-particle model. The total γ width is here

$$\Gamma_\gamma(J_i,E_i)=C\int_0^{E_i}E_\gamma{}^3A^{2/3}\frac{\sum\rho_f(E_f,J_f)}{\rho_i(E_i,J_i)}\,dE_f, \tag{A8}$$

where $E_\gamma = E_i - E_f$ and the summation is over spin values J_f from $|J_i - 1|$ to $J_i + 1$. The numerical value of the factor C depends on assumptions made in evaluating the integral of a radial wave function. Calculations of C commonly give values of Γ_γ which are in disagreement with observed values, and we therefore treat C as an empirical constant, chosen to fit experimental widths $\Gamma_\gamma(B_n)$, measured at the neutron binding energy. The evaluation of Eq. (A8) is simplified by the fact that for the small spin changes involved in dipole emission, the spin-dependent terms in the level density cancel to a good approximation (giving a factor of 3 from the summation over J_f), and only the spin-dependent part of the level density need be considered. Thus we have

$$\Gamma_\gamma(E_i) = 3C \int_0^{E_i} E_\gamma^3 A^{2/3} \frac{\rho_f(E_f)}{\rho_i(E_i)}\, dE_f . \tag{A9}$$

The level densities $\rho(E)$ at the relatively low excitation energies involved here were evaluated using Eq. (A3).

The second approach to the calculation of Γ_γ and its dependence upon energy is based on the application of the reciprocity theorem to the inverse γ-capture cross section, $\sigma(E_\gamma)$. The total γ width is then[22]

$$\Gamma_\gamma(E_i) = \frac{1}{\pi^2 \hbar^2 c^2 \rho(E_i)} \int_0^{E_i} E_\gamma^2 \rho_f(E_f) \sigma_A(E_\gamma) dE_\gamma . \tag{A10}$$

The giant-dipole-resonance model was used to determine the capture cross section $\sigma_A(E_\gamma)$. According to Axel,[23]

$$\sigma_A(E_\gamma) = \frac{1.3A}{100\Gamma_\gamma} \frac{E_\gamma^2 \Gamma_g^2}{(E_r^2 - E_\gamma^2)^2 + E_\gamma^2 \Gamma_g^2}. \tag{A11}$$

Here E_r and Γ_g are the resonance energy and total width of the giant dipole resonance. Values adopted for ^{61}Ni were $E_r = 17.8$ MeV[24] and $\Gamma_g = 5.0$ MeV.[25] The level density in Eq. (A10) was evaluated using Eq. (A3).

The energy dependences of $\Gamma_\gamma(E_i)$ as found from the two calculations were closely identical. The actual calculations were based on widths from Eq. (A9), normalized to $\Gamma_\gamma(B_n)$. The normalization values were based on values tabulated by Lynn,[26] inferring widths for the nuclei of interest from the tabulated values for neighboring nuclei. The adopted values were 300, 673, 1000, 350, and 90 meV, for ^{25}Mg, ^{57}Fe, ^{61}Ni, ^{91}Zr, and ^{119}Sn, respectively.

D. Neutron Widths

The partial width for neutron decay of CN_i to a discrete final state of spin J_f and excitation energy E_f is

$$\Gamma_n(E_i, J_i, \pi_i, E_f, J_f, \pi_f) = \frac{1}{2\pi} \frac{T'(J_i, E_n, J_f)}{\rho(U_i, J_i, \pi_i)}, \tag{A12}$$

where $E_n = E_i - E_f - B_n$ and $\rho(U_i, J_i, \pi_i) = \frac{1}{2}\rho(U_i, J_i)$. The transmission factor T' is defined in the same manner as T in Eq. (A7), but includes only l values which conserve parity. For ^{25}Mg, ^{57}Fe, and ^{61}Ni, $\rho(U_i, J_i, \pi_i)$ was calculated using Eq. (A4), with a normalization based on values of $\rho(B_n, 0)$ for states of one parity, tabulated by Lynn.[27] For ^{57}Fe and ^{61}Ni these are 18 and 21 MeV^{-1}, respectively. For ^{25}Mg an interpolated value of 1.5 MeV^{-1} was inferred from values for neighboring nuclei. For ^{91}Zr and ^{119}Sn the energy dependence of $\rho(U_i, J_i, \pi_i)$ was calculated from Eq. (A2), with a normalization to values of $\rho(B_n, 0)$ from Lynn of 110 and 2800 MeV^{-1}, respectively.

E. Neutron Fractional Yield

The neutron fractional yield from initial states (E_i, J_i, π_i) to a single final state (E_f, J_f, π_f) is then

$$f_n(E_i, J_i, \pi_i, E_f, J_f, \pi_f) = \frac{\Gamma_n(E_i, J_i, \pi_i, E_f, J_f, \pi_f)}{\Gamma_\gamma(E_i) + \sum \Gamma_n}, \tag{A13}$$

where Γ_n is found from Eq. (A12) and Γ_γ from Eq. (A9). The summation in the denominator is over all final states following neutron emission from CN_i. The calculated widths in Eq. (A13) are average widths, and thus the procedure outlined above gives

$$f_n = \frac{\bar{\Gamma}_n}{\bar{\Gamma}_\gamma + \bar{\Gamma}_n}. \tag{A14}$$

However, for decaying states lying slightly above the neutron binding energy, the neutron widths are distributed according to the Porter-Thomas distribution.[28] Thus the quantity of interest is

$$\langle f_n \rangle = \left\langle \frac{\Gamma_n}{\bar{\Gamma}_\gamma + \sum \Gamma_n} \right\rangle, \tag{A15}$$

where the average is taken over the Porter-Thomas distribution for neutron widths. While the general case described by Eq. (A15) is difficult to treat, the evaluation of Eq. (A15) was greatly simplified by exploiting the fact that, for given J_i, neutron emission to a specific final state usually received significant competition either from only one other neutron channel or from γ emission alone. Calculations made on this simplified basis gave corrected values $\langle f_n \rangle$, differing from f_n of Eq. (A14) by about 5 to 10%. The fractional yields $F_n(E_i, E_f, J_f, \pi_f)$ were calculated from Eqs. (A1) and (A5) using $f_n(E_i, J_i, \pi_i, E_f, J_f, \pi_f)$ defined by Eq. (A15).

*Work supported in part by the U. S. Atomic Energy Commission.

† Present address: Sloan-Kettering Cancer Research Institute, New York, New York.

‡ Present address: Stanford University, Stanford, California.

§ Present address: University of Alberta, Edmonton, Alberta, Canada.

[1]J. R. Grover, Phys. Rev. 123, 267 (1961); 127, 2142 (1962).

[2]J. R. Grover and J. Gilat, Phys. Rev. 157, 802, 814 (1967).

[3]J. F. Mollenauer, Phys. Rev. 127, 867 (1962).

[4]D. Sperber, Phys. Rev. 141, 927 (1966).

[5]D. G. Sarantites and B. D. Pate, Nucl. Phys. A93, 545 (1967).

[6]B. L. Cohen, E. C. May, T. M. O'Keefe, C. L. Fink, and B. Rosner, Phys. Rev. Letters 21, 226 (1968).

[7]B. L. Cohen, C. L. Fink, J. C. Van der Weerd, and R. J. Petty, Phys. Rev. C 1, 1237 (1970).

[8]H. Liskien and A. Paulsen, Nucl. Instr. Methods 69, 70 (1969).

[9]I. J. Taylor and J. Kalyna, Nucl. Instr. Methods 88, 267 (1970); V. V. Verbinski, W. R. Burrus, T. A. Love, W. Zobel, and N. W. Hill, *ibid*. 65, 8 (1968); F. T. Kuchnir and F. J. Lynch, IEEE Trans. Nucl. Sci. NS-15, No. 3, 107 (1968).

[10]F. S. Goulding, D. A. Landis, J. Cerny, and R. H. Pehl, Nucl. Instr. Methods 31, 1 (1964).

[11]S. Raman, *Nuclear Data Sheets* for $A = 60$, Nucl. Data B2(No. 5), 45 (1968); C. Moazed, T. Becker, P. A. Assimakopoulos, and D. M. Van Patter, Nucl. Phys. A169, 651 (1971).

[12]D. Bodansky, Ann. Rev. Nucl. Sci. 12, 79 (1962).

[13]M. Blann and G. Merkel, Phys. Rev. 131, 764 (1963); F. W. Pement and R. L. Wolke, Nucl. Phys. 86, 429 (1966).

[14]T. D. Thomas, Ann. Rev. Nucl. Sci. 18, 343 (1968); J. R. Huizenga, L. Vaz, F. C. Williams, Jr., and M. Blann, University of Rochester Report No. UR-NSRL-28, 1970 (unpublished); S. M. Grimes, J. D. Anderson, J. W. McClure, B. A. Pohl, and C. Wong, Phys. Rev. C 3, 645 (1971); and private communication.

[15]This led to a misleading statement on the angular dependence of the neutron yield in an early report on this work: C. Ling, D. Bodansky, J. R. Calarco, J. M. Cameron, and D. C. Chamberlin, Bull. Am. Phys. Soc. 16, 625 (1971).

[16]K. H. Bray, S. N. Bunker, M. Jain, K. S. Jayaraman, G. A. Moss, W. T. H. Van Oers, D. O. Wells, and Y. I. Yu, Phys. Rev. C 3, 1771 (1971).

[17]For somewhat similar analyses see, for example, Refs. 1 and 5, and E. R. Parkinson, Ph.D. thesis, University of Washington, 1965 (unpublished).

[18]A. Gilbert and A. G. W. Cameron, Can. J. Phys. 43, 1446 (1965).

[19]T. Ericson, Advan. Phys. 9, 425 (1960).

[20]C. M. Perey and F. G. Perey, Phys. Rev. 132, 755 (1963).

[21]J. E. Lynn, *The Theory of Neutron Resonance Reactions* (Clarendon Press, Oxford, 1968), Chap. VII.

[22]A. M. Lane and J. E. Lynn, Nucl. Phys. 11, 646 (1959).

[23]P. Axel, Phys. Rev. 126, 671 (1962).

[24]R. Bach and C. Werntz, Phys. Rev. 173, 958 (1968).

[25]E. Hayward, in *Nuclear Structure and Electromagnetic Interactions*, edited by N. MacDonald (Plenum, New York, 1965), p. 173.

[26]J. E. Lynn, *The Theory of Neutron Resonance Reactions* (see Ref. 21), p. 314.

[27]J. E. Lynn, *The Theory of Neutron Resonance Reactions* (see Ref. 21), p. 109.

[28]C. E. Porter and R. G. Thomas, Phys. Rev. 104, 483 (1956).